Ceramics International 43 (2017) 11260–11264

Contents lists available at ScienceDirect

Ceramics International

journal homepage: www.elsevier.com/locate/ceramint

Highly porous α-Al_2O_3 ceramics obtained by sintering atomic layer deposited inverse opals

Kaline P. Furlan[a,*], Robert M. Pasquarelli[a], Tobias Krekeler[b], Martin Ritter[b], Robert Zierold[c], Kornelius Nielsch[c], Gerold A. Schneider[a], Rolf Janssen[a,*]

[a] Institute of Advanced Ceramics, Hamburg University of Technology (TUHH), Denickerstraße 15, 21073 Hamburg, Germany
[b] Electron Microscopy Unit (BeEM), Hamburg University of Technology (TUHH), Eißendorfer Straße 42, 21073 Hamburg, Germany
[c] Institute of Nanostructure and Solid State Physics, Universität Hamburg, Jungiusstraße 11B, 20355 Hamburg, Germany

ARTICLE INFO

Keywords:
A. Sintering B. Electron microscopy B. Porosity D. Al_2O_3

ABSTRACT

A process for generating highly porous α-Al_2O_3 ceramics has been developed. In this paper, a combination of self-assembly and atomic layer deposition is demonstrated as a means to fabricate inverse alumina opals, which have their structures transformed via sintering. The resulting highly porous structure is stable even after a 4 h dwell time at 1400 °C, in contrast to structures generated by conventional powder metallurgy, sol-gel or colloidal powder suspension infiltration methods. TEM analysis reveals that the structure consists of single grain domains of up to 3 μm, each containing a randomly interconnected network of alumina ligaments that share a common crystalline orientation, suggesting a different mechanism of grain boundary migration during sintering. These highly porous α-alumina ceramics are considered to be ideal for filtration or catalysis applications.

1. Introduction

When compared to bulk ceramics, porous ceramic materials present many interesting properties such as low thermal conductivity, low density, high permeability and high surface area. When compared to other materials, such as metals and polymers, they also present longer lifetimes, constant filter quality, and high chemical, microbiological and thermal stability [1]. The most common materials used for porous ceramics are alumina, zirconia, titania and silica [2]. Among their applications are filters, catalysts supports, bioreactors, light weight components, thermal insulators, sensors and bone substitutes [1,3–10]. Their properties are dependent on the size, distribution and morphology of pores, as well as their interconnectivity. Therefore, the development of materials with controlled and narrow pore size distribution plus high surface area is of great interest [4].

There are several ways to fabricate porous ceramics, such as the replica technique, sacrificial template method, direct foaming and lastly the molding and sintering of sol-gel powders [1,2,9]. These methods provide a variety of porosity ranges; however, their distribution over the volume is hardly controlled. More recently, some other methods have gained attention, such as sol-gel infiltration of ordered structures, also referred to as colloidal crystals or direct opals, with metal nitrate precursors [11–16] or powder colloidal suspensions [13,17]. These methods produce YSZ [13,17], titania [15,16], zirconia [16], silica [15] and alumina [11,12,16] ordered macroporous ceramics after calcination. Additionally, atomic layer deposition (ALD) has recently been used to produce titania [18,19] and alumina [20] inverse opals for photonic applications. The possibility of strict thickness control on an Å-scale and surface-limited reactions are some advantages of an ALD route.

In the present work, we demonstrate a new technique for the development of highly porous ceramics, which exhibit fewer grain boundaries when compared with conventional formed structures. The material is produced by atomic layer deposition infiltration of a self-assembled PS colloidal crystal structure, which is first calcinated to generate an inverse alumina opal and later sintered to yield the desired porous and networked structure. The resulting highly porous α-alumina ceramics are considered to be ideal for filtration or catalysis purposes.

2. Material and methods

Monodisperse polystyrene (PS) particles (Microparticles GmbH) with diameter of 0.75 ± 0.02, 0.76 ± 0.02, 1.03 ± 0.04 and 1.50 ± 0.04 μm were self-assembled onto cleaned (Mucasol, Brand, Merz Hygiene GmbH) single-crystal sapphire substrates (randomly oriented,

* Corresponding authors.
E-mail addresses: kaline.furlan@tuhh.de (K.P. Furlan), janssen@tuhh.de (R. Janssen).

http://dx.doi.org/10.1016/j.ceramint.2017.05.176
Received 28 February 2017; Received in revised form 25 May 2017; Accepted 25 May 2017
Available online 26 May 2017

Crystec GmbH). Typical vertical convective self-assembly was performed within Teflon™ beakers containing suspensions of PS (0.8, 0.8, 0.9 and 1.0 mg/ml respectively according to the PS particle size) in deionized water. The beakers were kept inside a humidity chamber (HCP108, Memmert GmbH) at 70% relative humidity for 72 h at 55 °C.

A low-temperature ALD process was used to infiltrate the resulting PS templates with alumina. The precursors trimethylaluminium (TMA, Sigma Aldrich) and deionized water were used in a Savannah™ 200 reactor (Ultratech/Cambridge Nanotech) under exposure mode with a constant purge flow of nitrogen (30 sccm). The sample temperature was kept at 95 °C, below the glass transition temperature of the PS. Precursors were alternated with 0.2, 60 and 90 s of pulse, exposure and pump times, respectively. An average growth rate of 1.7 Å/cycle (TMA +water) was achieved. After ALD, the PS template was removed by heat treatment in air at 500 °C for 30 min, resulting in an inverse opal structure.

The inverse opals were then heat treated in air in a tubular furnace at a 5 °C/min heating rate until the desired temperature and dwell time were achieved. Sintering was performed at 1200 °C for 1 h, then at 1300 °C for 1, 3 and 4 h, and lastly at 1400 °C for 1, 3 and 4 h. After each heat treatment, the morphologies of the resulting structures were investigated by scanning electron microscopy (SEM, Zeiss Supra 55 VP). For the sample treated at 1400 °C/4 h, parts of the sample were crushed, dispersed in ethanol by ultrasonication and transferred to a carbon-coated grid for TEM imaging and selected-area electron diffraction (SAED) (TEM, Jeol JEM-2000FX-II).

3. Results and discussion

The typical appearance of an alumina inverse opal with a wall thickness of approximately 50 nm is shown in Fig. 1a (from surface top view) and Fig. 1b (in cross-section). This shell-like, FCC-ordered structure is achieved after burn-out of the PS template at 500 °C for 30 min and consists of three-dimensionally highly-ordered pores, which are interconnected through contact windows of adjacent PS spheres. Assuming that all of the structure is assembled under FCC packing, this means that ~74% of the whole structural volume is converted into macropores after the PS burn-out. Furthermore, from the SEM images, it is apparent that there are also nanopores located at the interstitial sites (either tetragonal or octahedral). This was attributed to the precursor reach and partial filling during the ALD process.

The influence of increasing the sintering temperature and time on the inverse opal structures can be seen in Fig. 1c-i. The opal heat treated at 1200 °C/1 h (Fig. 1c) did not show any significant structural change visible under SEM, and the ordering of the shells is still retained. However, it is already possible to visualize some line-like features spreading over the surface and through the opal. It is unclear whether these lines are grain boundaries, as in our previous work with titania inverse opals [18], or cracks generated due to retraction associated to the alumina α phase transition (as some of the lines are continuous over the shells) or both. X-ray diffraction measurements show that this temperature indeed coincides with the transformation to α-alumina (Fig. S1 in Supplementary information). The results are in agreement with the studies performed by Zhang et al. [21] and Lampert et al. [22] in ALD alumina structures. However, the temperature is notably lower than that reported by Rani and Sahare [23,24] for sol-gel structures and entirely different from the report by Waterhouse et al. [12], in which several transitions aluminas (γ,δ,θ) are formed before it transforms to α-alumina at 1200 °C.

Subsequent sintering at 1300 °C/1 h reveals the opening of these lines, thus supporting the cracks hypothesis. Further increase in sintering time showed interconnection and widening of these openings, as well as the continuous flattening of the surface topology of the shell-like structure. After 8 h, only some isolated points can be identified as the initial spherical shells.

After sintering at 1400 °C for 4 h (Fig. 1h), the structure evolves into a filter-like structure, in which the original shell structure can no longer be identified. This vermicular structural occurrence in alumina sintering is well-known and earlier reported by many other authors [1–4,6,9,10,25–27]. However, for the samples described in this paper, the structure is stable over time and remains practically unchanged after sintering at 1400 °C for a total of 8 h (Fig. 1i). This is in contrast to results obtained, for example, by Dutta et al. [27] for sintering sol-gel generated alumina deposited also on the top of sapphire. They reported a vermicular structure formation during sintering but instead observed coarsening of the microstructure after 6 h at 1400 °C with clear densification and pronounced porosity reduction. The same occurred in alumina structures generated by inkjet 3-D printing and sintered at 1400 °C for 4 h [1], where additional undesired abnormal grain growth generated coarse grains of approximately 100 μm.

The results of this work also differs from those obtained in the sintering of alumina and YSZ opals produced by infiltration of sol-gel [11–13,17] and powder colloidal suspensions [17]. In the case of Waterhouse et al. [12], crystallites and grain boundaries are already identified after heating at 550 °C for 4 h in a sample where γ-alumina is identified by XRD. Sokolov et al. [11] performed heat treatments at higher temperatures (1300 °C/4 h), for which the vermicular structure also occurred, but they heated the samples no further. Crystallites of 50–100 nm are also clearly identified for YSZ direct opals after heating at 1100 °C/5 h [13].

The nature of these differences may be attributed to our starting structure and its evolutionary pathway. It is important to point out that, unlike previously noted structures developed by sol-gel or powder colloidal suspension infiltration, the production of opals by atomic layer deposition results in the presence of additional nanopores at the interstitial sites (tetragonal or octahedral), due to the limit of the precursor to reach and fill those areas. Therefore, the inverse opals developed in this work have a larger pore volume fraction (are more porous) than the previously referenced opals. Additionally, the resulting shell-like structure with hollow nodes contains a very homogenous distribution of ceramic material. This is in contrast to more traditional opals produced by sol-gel of powder colloidal infiltration, which are less homogeneous and may also exhibit more gradients in chemical composition and more transient stresses than the opals produced by ALD.

Lastly, the differences could be attributed to the fact that the inverse opal structure described in this work is fully amorphous after ALD deposition, thus needing nucleation sites for crystallite formation and time for further growth. In the case of our structures, the nucleation sites amount shall be limited by the shell size thickness and the growth spatially restricted by along a few definite paths. As demonstrated by Yadlovker and Berger [28], the nucleation and growth cannot take place in areas smaller than the critical nuclei radius. For our structures this would coincide with areas where the shell thickness is thinner than the critical radius. Furthermore, where pores are present, either the macropores (original PS particles sites) or nanopores (interstitial sites) nucleation will off course not happen.

The mechanisms of sintering in polycrystalline ceramic materials are defined by the diffusional transport of matter along definite paths. The most important densifying mechanisms in this case are grain boundary diffusion and lattice diffusion from the grain boundary to the pore [29]. These densification mechanisms occur when the distance between the crystallites centers are reduced. On the other hand, the formation or existence of pores leads to an increase in this distance, inhibiting densification in some orientation, resulting in a vermicular structure. Under these conditions, neck growth occurs without further

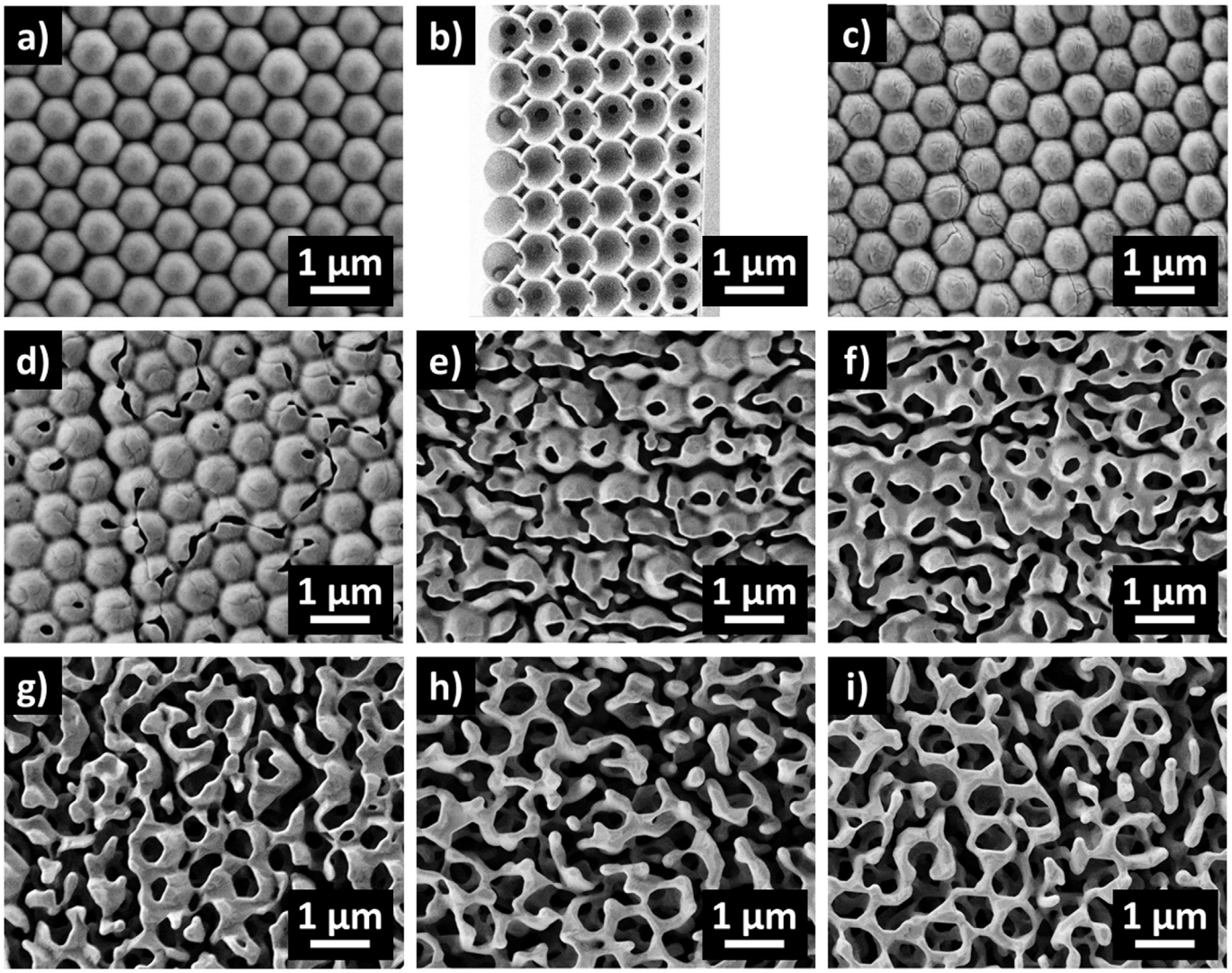

Fig. 1. SEM images of inverse opal structures as a function of heat treatment – (a) top view and (b) cross section after 500 °C for 30 min and top view after (c) 1200 °C/1 h, (d) 1200 °C/1 h+1300 °C/1 h, (e) 1200 °C/1 h+1300 °C/4 h, (f) 1200 °C/1 h+1300 °C/8 h, (g) 1200 °C/1 h+1300 °C/8 h+1400 °C/1 h, (h) 1200 °C/1 h+1300 °C/8 h+1400 °C/4 h and (i) 1200 °C/1 h+1300 °C/8 h+1400 °C/8 h.

densification [30]. In the case of the ceramic materials developed in this paper, the pores are an intrinsic part of the initial shell structure. For the reasons cited above, instead of neck growth and pore elimination, which usually happen in classic particle sintering, crystallite growth and enlargement of pore connection is found. Nevertheless, the formation of highly-curved, still-smoothed networks with large single crystalline domains cannot be explained by classical sintering theory, which states that highly curved interfaces should be reduced or at least smoothed [31]. In our previous work with titania inverse opals [18], we showed that during sintering, the struts of the structure (in between pores, connections of the shells) grew at the expense of the shell curvature. It is possible that for this work that the struts grew over to form the greater crystallites seen under TEM analysis. In an overall view, the whole structure seems to de-sinter.

In contrast to coalescence, in which small particles shrink and large nodes grow, a vermicular structure occurs when grain boundaries are removed through the network of particles, forming worm-like single grains. In the case of an inverse opal, pre-existing pathways are provided by the structure itself. In order to assess the extent of vermicular features produced in this work, broken fragments of the sample treated at 1400 °C for 4 h were characterized using TEM. TEM analysis shows that the vermicular structure consists of a randomly interconnected network of alumina ligaments with a varying diameter (80–350 nm), as shown by the representative bright-field image in Fig. 2. The imaged structure shows fracture faces marked with arrows, indicating even larger feature sizes in the bulk material. SAED experiments on the marked areas show the expected reflexes of α-alumina ($R\bar{3}c$ SG. 167) in the zone axis $[\bar{3}12\bar{1}]$. All diffraction patterns in Fig. 3 were recorded without changing the tilt of the sample, revealing a large grain size of at least 3 µm with only negligible orientation change inside the grain, leading to the asymmetric intensity distribution around the primary beam of the diffraction patterns. To gain a sense of scale in the structure, a grain size of ~3 µm is roughly 4-fold larger than the original PS-templated pores. The blue marked SAED experiment resulted in an off-axis crystal orientation, indicating a grain boundary somewhere between the red and blue marked areas.

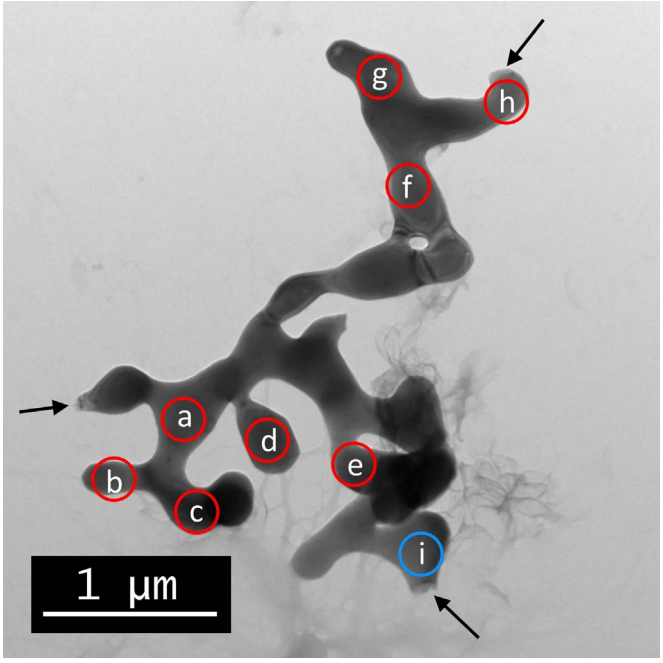

Fig. 2. TEM BF-image of sintered alumina inverse opal (1400 °C). Arrows indicate fracture faces, colored marks correspond to SAED experiments in Fig. 3.

Additional investigations showed that the desired structure can be achieved also by heat treatment at 1200 °C/1 h + 1400 °C/4 h (Fig. 4). Furthermore, it was found that the openness of the structure (Fig. 4a-c) can be easily varied by the straight-forward modification of the initial PS template size during the self-assembly step and shell thickness, without any need for further process modifications. This is an advantage when comparing ALD-inverse opals with alumina opals generated by boehmite sol-gel, as several reconstructive phase transformations and dehydration during heat treatment in addition to the initial morphology and particle size of boehmite can affect the final porosity [26], resulting in a nonlinear relation and thus a not straight-forward predictable structure. One should note that these are initial and very interesting findings that we intend to communicate to the materials science society. Further investigations in order to strength our understanding of these new structures are ongoing.

4. Conclusions

A new method for production of highly porous ceramic materials with large domains of identical crystalline orientation has been developed. The structures simultaneously exhibit an open cell morphology, which is expected to provide high surface area. However, textural properties need to be measured and verified. The structure also has few grains boundaries, thereby providing advanced thermal stability and, most likely, corrosion resistance. The synthesis comprises the infiltration of a self-assembled structure by atomic layer deposition and subsequent heat treatment, which

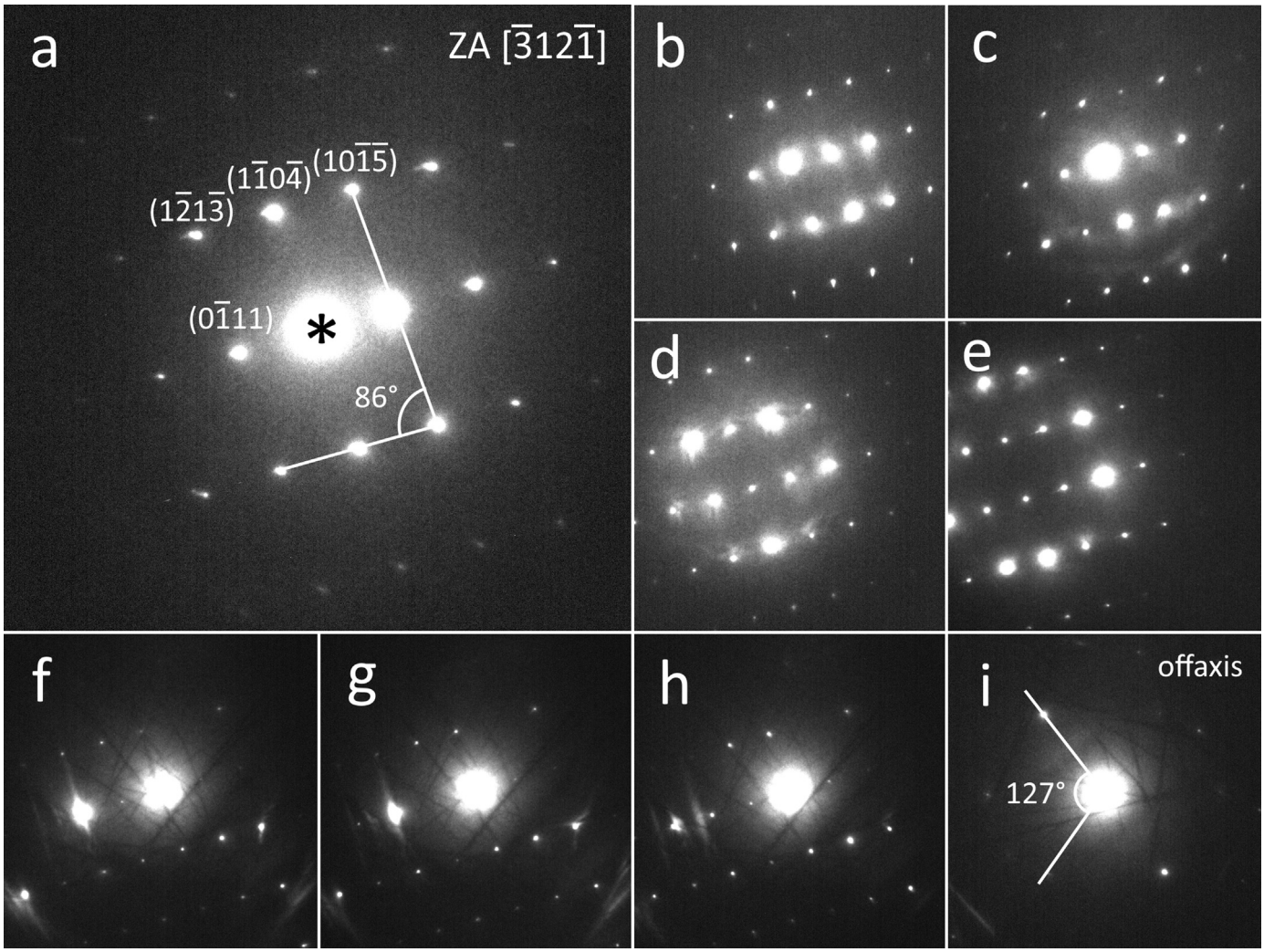

Fig. 3. SAED patterns of different points in the sample, matching the α-alumina pattern (ZA [$\bar{3}12\bar{1}$]).

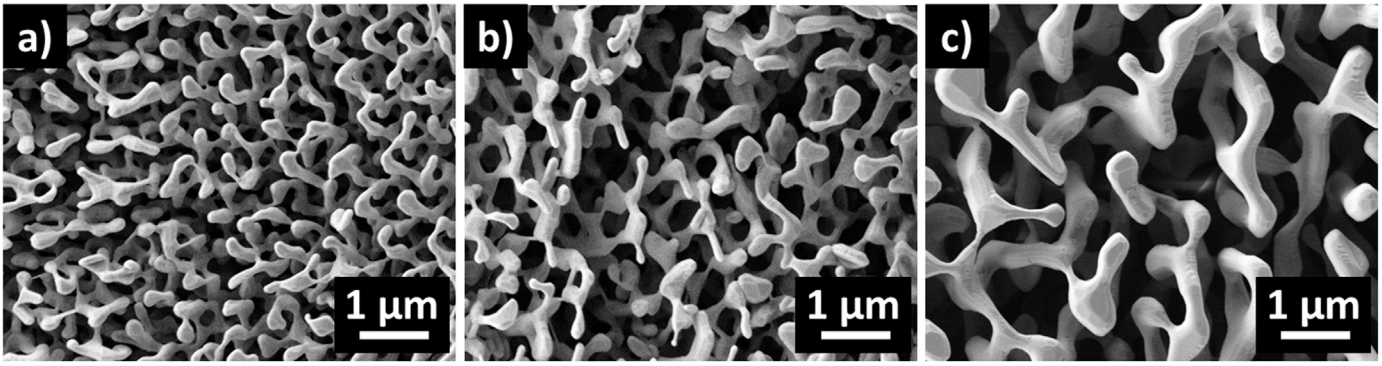

Fig. 4. SEM images of inverse opal structures according to initial PS sphere sizes of (a) 0.75 µm, (b) 1.03 µm and (c) 1.50 µm, with ALD-shell thickness of (a–b) 27 nm and (c) 82 nm shown after heat treatment at 1200 °C/1 h + 1400 °C/4 h.

yields an open, stable network with large vermicular domains of α-alumina. Tailorability of the structure by controlling the initial PS template size and shell thickness were demonstrated. Foreseeable applications include filters and catalysts with possible pore size tunability through modification of the initial PS spheres size.

Acknowledgements

The authors gratefully acknowledge financial support from the German Research Foundation (DFG) via SFB 986 "M^3", projects C3, C5 and Z3.

Appendix A. Supporting information

Supplementary data associated with this article can be found in the online version at http://dx.doi.org/10.1016/j.ceramint.2017.05.176.

References

[1] Z. Chen, N. Brandon, Inkjet printing and nanoindentation of porous alumina multilayers, Ceram. Int. 42 (7) (2016) 8316–8324.
[2] M. Barmala, A. Moheb, R. Emadi, Applying Taguchi method for optimization of the synthesis condition of nano-porous alumina membrane by slip casting method, J. Alloy. Compd. 485 (1–2) (2009) 778–782.
[3] R. Liu, Y. Li, C.-A. Wang, S. Tie, Fabrication of porous alumina–zirconia ceramics by gel-casting and infiltration methods, Mater. Des. 63 (2014) 1–5.
[4] M. Montero, T. Molina, M. Szafran, R. Moreno, M.I. Nieto, Alumina porous nanomaterials obtained by colloidal processing using D-fructose as dispersant and porosity promoter, Ceram. Int. 38 (4) (2012) 2779–2784.
[5] F. Tian, J. Lyu, J. Shi, F. Tan, M. Yang, A polymeric microfluidic device integrated with nanoporous alumina membranes for simultaneous detection of multiple foodborne pathogens, Sens. Actuators B: Chem. 225 (2016) 312–318.
[6] H. Fang, J.F. Gao, H.T. Wang, C.S. Chen, Hydrophobic porous alumina hollow fiber for water desalination via membrane distillation process, J. Membr. Sci. 403–404 (2012) 41–46.
[7] S.-J. Li, Y. Xing, M.-Y. Tang, L.-H. Wang, L. Liu, A novel nanomachined flow channel glucose sensor based on an alumina membrane, Anal. Methods 5 (24) (2013) 7022–7029.
[8] T. Di Costanzo, A.A. Fomkin, C. Frappart, A.N. Khodan, D.G. Kuznetsov, L. Mazerolles, D. Michel, A.A. Minaev, V.A. Sinitsin, J.L. Vignes, New method of porous oxide synthesis: alumina and alumina based compounds, Mater. Sci. Forum 453–454 (2004) 315–322.
[9] S. Li, C.-A. Wang, J. Zhou, Effect of starch addition on microstructure and properties of highly porous alumina ceramics, Ceram. Int. 39 (8) (2013) 8833–8839.
[10] T. Nagaoka, T. Tsugoshi, Y. Hotta, K. Sato, K. Watari, Fabrication of Porous Alumina Ceramics by New Eco-Friendly Process, J. Ceram. Soc. Jpn. 113 (1313) (2005) 87–91.
[11] S. Sokolov, D. Bell, A. Stein, Preparation and Characterization of Macroporous α-Alumina, J. Am. Ceram. Soc. 86 (9) (2003) 1481–1486.
[12] G.I.N. Waterhouse, W.-T. Chen, A. Chan, H. Jin, D. Sun-Waterhouse, B.C.C. Cowie, Structural, Optical, and Catalytic Support Properties of γ-Al 2 O 3 Inverse Opals, J. Phys. Chem. C. 119 (12) (2015) 6647–6659.
[13] A. Lashtabeg, J. Drennan, R. Knibbe, J.L. Bradley, G.Q. Lu, Synthesis and characterisation of macroporous Yttria Stabilised Zirconia (YSZ) using polystyrene spheres as templates, Microporous Mesoporous Mater. 117 (1–2) (2009) 395–401.
[14] C.F. Blanford, H. Yan, R.C. Schroden, M. Al-Daous, A. Stein, Gems of Chemistry and Physics: macroporous Metal Oxides with 3D Order, Adv. Mater. 13 (6) (2001) 401–407.
[15] B.T. Holland, Synthesis of macroporous minerals with highly ordered three-dimensional arrays of spheroidal voids, Science 281 (5376) (1998) 538–540.
[16] B.T. Holland, C.F. Blanford, T. Do, A. Stein, Synthesis of highly ordered, three-dimensional, macroporous structures of amorphous or crystalline inorganic oxides, phosphates, and hybrid composites, Chem. Mater. 11 (3) (1999) 795–805.
[17] A. Lashtabeg, J.L. Bradley, G. Vives, J. Drennan, The effects of templating synthesis procedures on the microstructure of Yttria Stabilised Zirconia (YSZ) and NiO/YSZ templated thin films, Ceram. Int. 36 (2) (2010) 653–659.
[18] R.M. Pasquarelli, H.S. Lee, R. Kubrin, R. Zierold, A.Y. Petrov, K. Nielsch, G.A. Schneider, M. Eich, R. Janssen, Enhanced structural and phase stability of titania inverse opals, J. Eur. Ceram. Soc. 35 (11) (2015) 3103–3109.
[19] R. Kubrin, H.S. Lee, R. Zierold, A. Yu. Petrov, R. Janssen, K. Nielsch, M. Eich, G.A. Schneider, J. Ballato, Stacking of Ceramic Inverse Opals with Different Lattice Constants, J. Am. Ceram. Soc. 95 (7) (2012) 2226–2235.
[20] M. Knez, K. Nielsch, L. Niinistö, Synthesis and surface engineering of complex nanostructures by atomic layer deposition, Adv. Mater. 19 (21) (2007) 3425–3438.
[21] L. Zhang, H.C. Jiang, C. Liu, J.W. Dong, P. Chow, Annealing of Al_2O_3 thin films prepared by atomic layer deposition, J. Phys. D: Appl. Phys. 40 (12) (2007) 3707.
[22] L.F. Lampert, A. Barnum, S.W. Smith, J.F. Conley, J. Jiao, Phase transitions and in situ dynamics of crystal grain formation of alumina nanotubes templated by vertically aligned carbon nanotubes, RSC Adv. 5 (83) (2015) 68251–68259.
[23] G. Rani, P.D. Sahare, Effect of phase transitions on thermoluminescence characteristics of nanocrystalline alumina, Nucl. Instrum. Methods Phys. Res. Sect. B: Beam Interact. Mater. At. 311 (2013) 71–77.
[24] G. Rani, P.D. Sahare, Effect of temperature on structural and optical properties of boehmite nanostructure, Int. J. Appl. Ceram. Technol. 12 (1) (2015) 124–132.
[25] T.L. Hong, H.T. Liu, C.T. Yeh, S.H. Chen, F.C. Sheu, L.J. Leu, C.I. Wang, Electron microscopic studies on pore structure of alumina, Appl. Catal. A-Gen. 158 (1–2) (1997) 257–271.
[26] A.C. Zaman, C.B. Üstündağ, C. Kaya, Boehmite derived surface functionalized carbon nanotube-reinforced macroporous alumina ceramics, J. Eur. Ceram. Soc. 30 (12) (2010) 2525–2531.
[27] S. Dutta, T.B. Kim, T. Krentz, R.P. Vinci, H.M. Chan, Sol–gel-derived single-crystal alumina coatings with vermicular structure, J. Am. Ceram. Soc. 94 (2) (2011) 340–343.
[28] D. Yadlovker, S. Berger, Nucleation and growth of single crystals with uniform crystallographic orientation inside alumina nanopores, J. Appl. Phys. 101 (3) (2007) 34304.
[29] D.W. Richerson, Modern ceramic engineering: Properties, processing, and use in design / David W. Richerson, 2nd ed., M. Dekker, New York, N.Y, 1992.
[30] S.A. Hassanzadeh-Tabrizi, E. Taheri-Nassaj, Effects of milling and calcination temperature on the compressibility and sinterability of a nanocrystalline Al_2O_3 -$Y_3Al_5O_{12}$ composite powder, J. Am. Ceram. Soc. 91 (11) (2008) 3546–3551.
[31] L. Wang, J. Hu, Y. Cheng, Z. Fu, Z. Shen, Y. Xiong, Defect formation by order coalescence in vermicular grains during alumina phase transformation, Scr. Mater. 107 (2015) 59–62.